
Check for updates

...e of numerical parameters, ...ometric complexity or an assumption ...and its extent. There is some freedom in these ...parameters as for the given case it is not obvious what the most adequate parameters would be. Often the parameters are chosen more for convenience, for example to simplify the physics model or to achieve numerical convergence as quickly as possible. Sometimes, the modeller is tempted to oversimplify the model setup that neglect, unknowingly, some important aspects of the underlying physics.

For example, a typical edge modeller usually choses a SOL grid width that is at least wide enough to include the near-SOL heat decay length parameter λ_q. Sometimes there are also technical constraints that would not allow a SOL grid width to be wide enough to fully include λ_q and then one possible "workaround" is to reduce the level of complexity for the wall geometry (by removing or modifying edges and corners that would otherwise limit the SOL grid width). As we will show in this paper, such simplifications can have a significant impact on the overall numerical plasma solution. The interpretation of the model results in terms of physics can therefore be hampered, perhaps unknowingly. In this paper we discuss systematically the impact of a finite grid size (i.e. the SOL grid width) and the significance of the level of divertor geometric details on the overall SOLPS-ITER edge plasma solution. It will be shown that it is rather the shape of the density profile expressed through a near-SOL decay parameter λ_{ne} upstream (rather than λ_q) that defines the minimum required SOL grid width for the simulation.

A set of JET H-mode discharges with the ITER-like wall (ILW, tungsten plasma-facing components (PFCs) in the divertor, beryllium for the main-chamber) has been selected for modelling the inter-ELM phase. In the following subsection the experimental setup of the JET discharge is described and the SOLPS-ITER model setup is briefly sketched. The modelling results are presented and compared to the experimental data in Section 3. A discussion follows in Section 4 highlighting the question of interpretation of model results if one modifies fundamental numerical parameters in SOLPS-ITER like the SOL grid width or geometric details. Section 5 concludes the paper with a summary.

2. Experiment and model setup

As experimental basis for the presented numerical exercise well diagnosed JET-ILW H-mode experiments in unseeded conditions from the C30C JET campaign in 2012 had been chosen [6]. In this specific JET campaign a large number of identical plasmas in semi-horizontal divertor configuration had been repeated (Ip/Bt = 2.0MA/2.4T, low-δ, P_{NBI} = 11MW, deuterium feed-forward gas injection $1.0{\cdot}10^{22}$ s^{-1} into the high-field side (HFS) divertor) to achieve a total accumulated time of 900 s in H-mode at with $\Delta W_{ELM} \sim 160$ kJ ELMs at $f_{ELM} \sim 30$ Hz. The well diagnosed edge plasma conditions, for which a post-mortem analysis of the PFCs exists, are currently utilized for the analysis of Be/W transport in JET using the ERO2.0 code [7] requiring modelled background plasmas in 2D from SOLPS-ITER.

In the following, the JET plasma discharge #83712 stands as the reference discharge for the C30C campaign. The EFIT equilibrium was taken from this specific discharge, representing the proxy for all identical discharges from the 2 week period of the C30C JET campaign. Upstream n_e and T_e profiles were taken from coherently averaged high-resolution Thomson scattering profiles (HRTS) across all C30C discharges. For having representative upstream conditions for the inter-ELM phase, only those data points shortly before the ELM event were taken into account in the averaging (i.e. the last 20–30% of the inter-ELM period). From the attached divertor conditions and with the outer strike line positioned on the LFS horizontal target (c.f. Fig. 1) the evolution of surface temperature T_{surf} and perpendicular target heat fluxes q_{perp} were coherently averaged from the divertor IR camera (IRTV) system (again across all ELMs and discharges from C30C). Also the HFS recycling flux was measured from Langmuir probes averaged

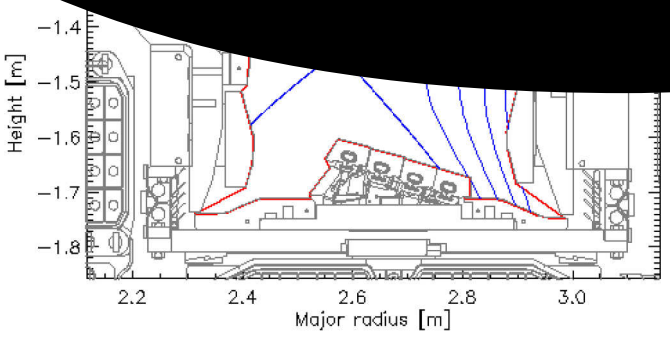

Fig. 1. Semi-horizontal divertor geometry setup of JET discharge #83712 representing a reference to all discharges executed during the C30C campaign. To guide the eye some SOL flux surfaces are displayed with a separation of 10 mm at the outer mid-plane. With poloidal flux expansion these flux surfaces increase their distance by a ~ factor 25–50 mm at the LFS target plate.

coherently and cross-checked with D_α & D_2 molecule spectroscopy. For further analysis of the inter-ELM phase the ELM transients have been removed in the signals (c.f. [8] for an in-depth analysis of the ELM-phase itself in C30C).

The SOLPS-ITER code [2,3] had been set up for a D-only single fluid plasma simulation with parallel transport (along field lines) assumed to be classical Spitzer with flux limiting corrections applied for electron heat and ion viscosity. Anomalous transport parameters were set to be spatially varying, including an edge transport barrier (ETB) represented by reduced particle diffusion and heat conductivities inside a narrow layer just inside the separatrix. The exact form of the transport parameter profiles for diffusion D_{edge} and heat conductivities $\chi^{e,i}_{edge}$ had been chosen by executing a fitting procedure to match the n_e and T_e pedestal profiles as well heat decay parameter in the near-SOL region upstream. For the latter a slight extension of the ETB into the SOL region was required (~0.4 cm). In the far-SOL transport was assumed to be comparably high with no spatial variation. Inside the divertor transport was assumed to be flat at increased level. In the current version of SOLPS-ITER the plasma is not in direct contact with the outer wall, hence a decay length of 3 cm was assumed for the plasma boundary conditions at the outer plasma grid edge. A quadratic correction for ballooning transport (increasing with major R) was included. Neither radial pinch-like convection nor drift effects were included in the present study. Boundary conditions were set to correspond to experimental values for heating at the core boundary and the gas-fueling rate into the HFS private flux zone was the same as in the experiment.

To assess the role of the grid size three different geometries had been setup (c.f. Fig. 2): case A) a grid with a regular, more narrow width of the SOL region technically limited by a small step-like structure of the LFS horizontal divertor plate, case B) the same as A but with a sloped extension of the LFS horizontal plate into the LFS corner region, and case C) a grid with a wide SOL plasma region to maximize the volume covered by the SOL plasma in the main-chamber; this requires the sloped extension of the LFS target plate into the corner as in B. In all 3 cases, the number of poloidal and radial cells had been kept constant, leading to a somewhat higher radial resolution of the grid in the SOL region for case A and B compared to C. For all 3 cases the radial grid extent of the SOL at the outer mid-plane is large enough to cover at least one heat decay length λ_q.

For the neutral transport modelled by EIRENE, an unstructured triangular mesh was overlaid on top of the plasma grid with each plasma cell being divided up into at least two triangular cells. One of the SOLPS-ITER options is the possibility to extend the triangular mesh for the neutrals into the remote regions in the poloidal plane. This is of specific importance as for JET the only accessible pressure gauge for

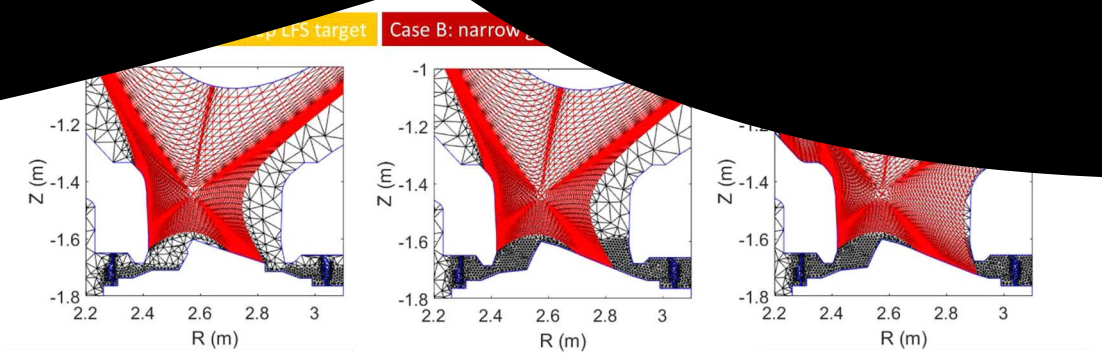

Fig. 2. The three different grid cases. The red grid represents the structured quadrangular plasma grid in SOLPS-ITER. Overlaid (in black) is the unstructured triangular mesh for the neutrals (EIRENE) including the cells for the plasma cells, each split into two triangles. Unlike the plasma grid the neutral triangular mesh is touch the outer wall. (For interpretation of the references to colour in this figure legend, the reader is referred to the web version of this article.)

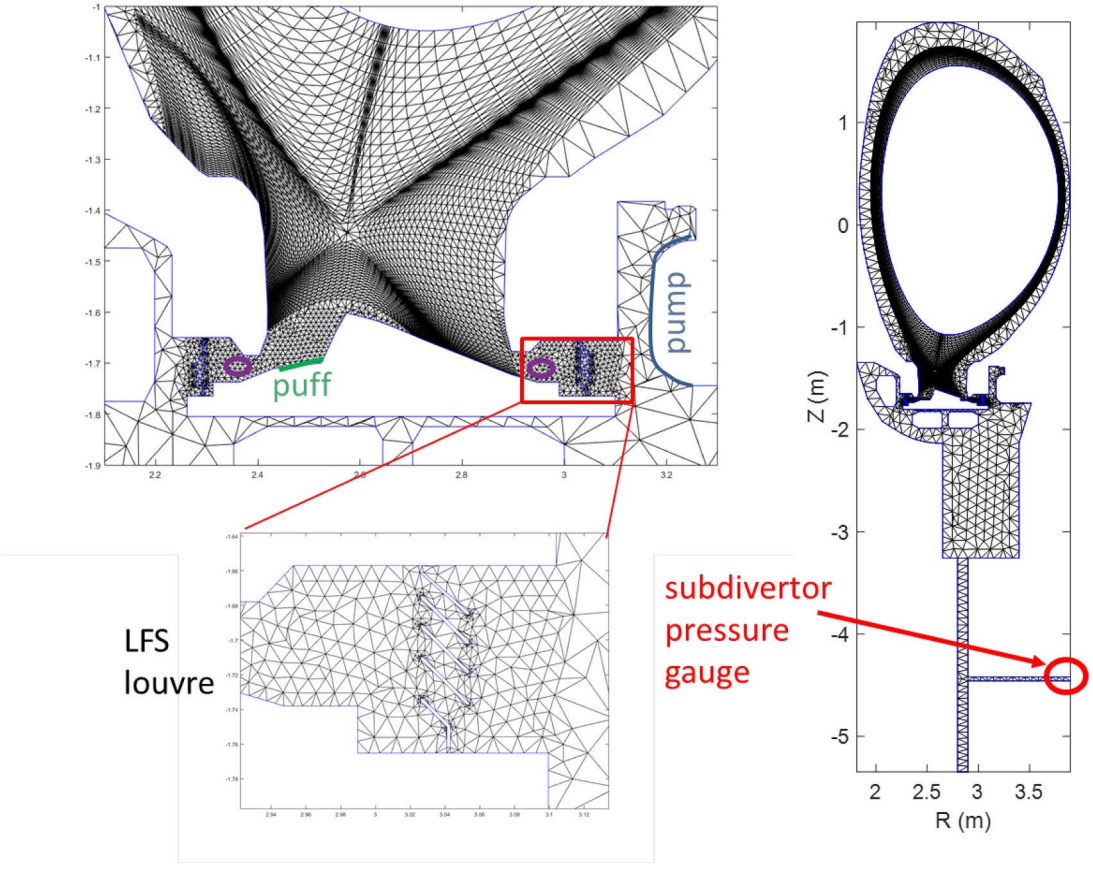

Fig. 3. The full unstructured triangular mesh including the structures for the sub-divertor, the louvre structures, the pump and puff location as well as the location of the single pressure gauge well below the divertor region.

matching the neutral pressure (an important model constraint [4]) is deep in the sub-divertor region. Also, small structures in the JET's louvre regions can be adequately represented (c.f. Fig. 3), leading to a significantly reduced flux of energetic atoms towards the pump region in the LFS as in the experiment. With the extended neutral grid option the pump structure itself and its pumping speed can be included in the model as well. The neutral physics model corresponded to the set of atomic and molecular database as generally described in [9]. However, with the divertor in attached conditions neutral viscosity effects could be treated as negligible: for the given attached (low-density) JET simulation case the optional BGK treatment of the neutral viscosity was tested with no dramatic change in the overall result for the plasma profiles (however, the molecular pressure in the divertor increased by a factor ~2 with the neutral viscosity included, c.f. also the discussion section below)

3. Results

In Fig. 4 the simulation cases are compared with the selected diagnostic data that constrained the model upstream and downstream. Case A has been taken as the first reference for which the profiles have been matched as close as possible to HRTS, Langmuir probe and IRTV data. As explained before the transport model in the other cases B and C are identical to A, with the exception of the grid extent in the SOL and/or geometrical details in the divertor. By taking case A as the reference, the simplified divertor geometry of the divertor (case B) has only a very

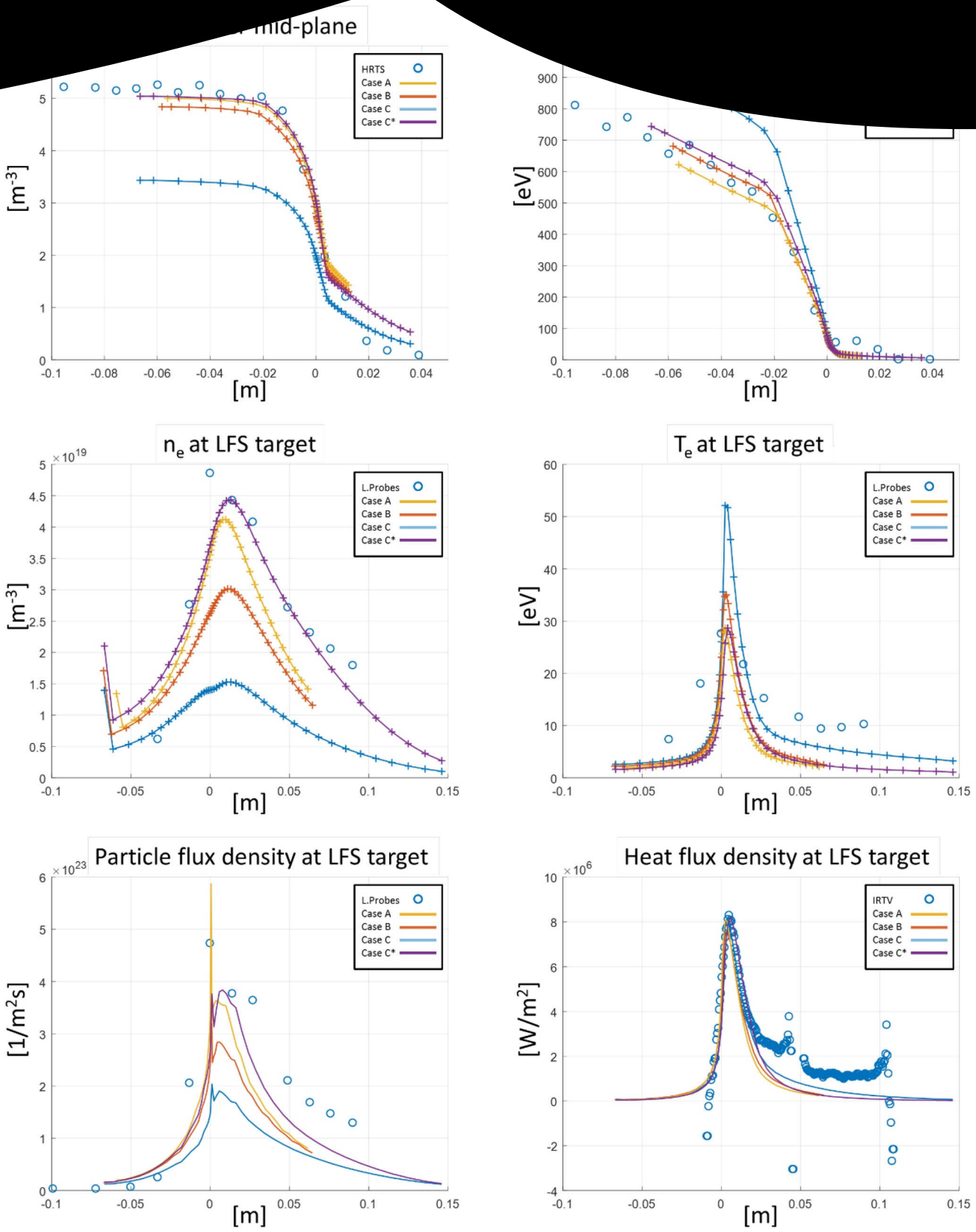

Fig. 4. Comparison of up- and downstream profiles experiment vs. model. The color code is as in Fig. 2 and represents the plasma grid variation and modification sin the divertor structure: case A narrow SOL grid width with step in LFS target plate (yellow), case B narrow SOL grid width with stretched LFS target slope (red), cases C (blue) and C* (purple) wide SOL grid width that technically requires the LFS target to be sloped. (For interpretation of the references to colour in this figure legend, the reader is referred to the web version of this article.)

...lines. The existence of the ... plate inside the neutral simulation ... outside the plasma grid) however leads to a ... increase of about 15% for target n_e and particle flux Γ_t.

When the width of the SOL grid is widened (case C) a significant decrease in upstream separatrix density n_e^{sep} (30%) is seen, concomitantly with a strong decrease of downstream n_e and Γ_t (65%). As a result of the reduced n_e^{sep} (driven by less neutrals fueling the core region) the top pedestal density n_e^{ped} is similarly reduced (30%) keeping the density gradient inside the ETB ∇n_e^{ETB} constant. However, with the core heat flux density and pedestal transport fixed in the code, ∇T_e^{ETB} (and thus also T_e^{ped}) must rise in response to a lower n_e^{ped}. In contrast T_e^{sep} varies much less significantly, a feature of the classical Spitzer's conductivity being not dependent on n_e but $\sim T_e^{5/2}$ and consistent with the two-point model prediction in attached conditions $T_e^{sep} \sim (q_{||}L_c/\kappa_{0e})^{2/7}$, with L_c connection length, κ_{0e} parallel electron conductivity. With the increased ∇T_e^{ETB} the parallel heat flux $q_{||} \sim P^{sep}/R_{maj}$ is increased. This however does not lead to a significant increase in T_e^{sep} due to its weak dependence on $q_{||}$, especially when moving from a high-recycling regime towards a more sheath limited regime at lower n_e^{sep}. The observed ~65% larger $T_{e,t}$ at the target plate must be to a large extent driven by the decrease of n_e^{sep} leading to a reduced $n_{e,t}$ and Γ_t (that is also understood from the two-point model prediction $T_t \sim (P^{sep})^2/(n_e^{sep})^3$). As a result the total plasma heat load density arriving perpendicular at the LFS target plate $q_{perp,t} \sim \gamma \Gamma_t T_{e,t}$ in case C is similar to case A/B (assuming constant sheath heat transmission factor γ in SOLPS-ITER) and remains also within the ballpark of 15% compared to the peak experimental IR data of $q_{perp,t}$.

For further analysis of the impact of the finite SOL grid width on the target heat flux, the experimental and numerical $q_{perp,t}$ profiles (along the target s-coordinate) have been deconvoluted adopting the Wagner/Eich fitting procedure [10,11]. Fig. 5 summarizes for the investigated cases and additional cases with modified transport and/or pumping albedo R (pumping speed). The values for the heat decay parameter $\lambda_{int}^{div} = \lambda_q^{div} + 1.64 \cdot S$ at the divertor entrance [12] and the numerically derived value for λ_q^{up} from the outer midplane heat flux profiles (derived from an exponential fit of $q_{||}$ at outer midplane) are compared with the experimentally measured quantities. SOLPS-ITER underestimates (5–25%) λ_{int}^{div} and a dependence on the SOL grid width is observed: λ_{int}^{div} is 20% larger in case C with the wide SOL grid width.

In order to match the upstream profiles also for the wide SOL grid case C, the ETB transport parameters have been modified (decrease of

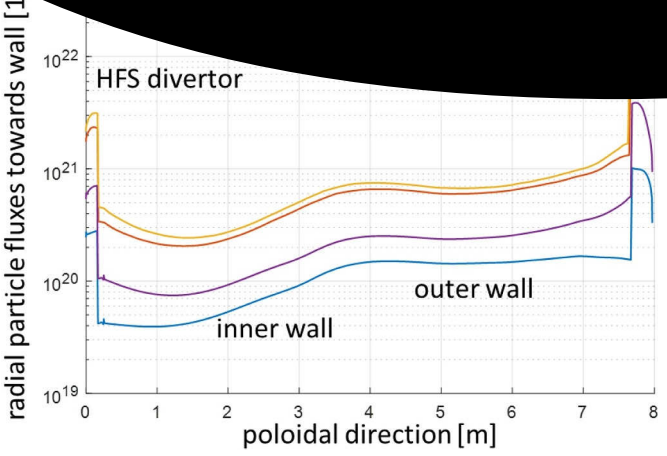

Fig. 6. Radial plasma outflow towards the walls (taken at the outermost plasma grid boundary not directly in touch with the walls), Color code as in Fig. 2 for cases A, B, C and C* (with the re-matched case C* in purple). (For interpretation of the references to colour in this figure legend, the reader is referred to the web version of this article.)

D^{ETB} by ~ factor 2, increase of $\chi_{e,i}^{ETB}$ by 15%, reduction of pumping speed (1-R) by ~ factor 3). In the following, this amended case is named as case C*. For the cases in which the upstream conditions/profiles for n_e and T_e are matched (cases A, B and C*) it is obvious that λ_q^{up} is barely affected by the divertor conditions: neither the SOL grid width nor a change in the pumping speed contribute to a change to λ_q^{up}. It is solely the transport assumption for the radial heat conduction which sets λ_q^{up} upstream.

Compared to the wide SOL grid case C/C* an extra cooling of the SOL further downstream is observed in case A/B with the narrow SOL grid width being reflected by a reduced ratio $\lambda_{int}^{div}/\lambda_q^{up}$ in case A/B (c.f. Fig. 5).

The radial particle fluxes towards the outer wall are also affected by the SOL grid width (c.f. Fig. 6). With the narrow grid (case A/B) the fluxes towards the wall are enhanced by a factor 4–5 compared to the wide grid case C. With the decay length fixed at the outer boundary the change in flux must be purely attributed to a proportionally change in

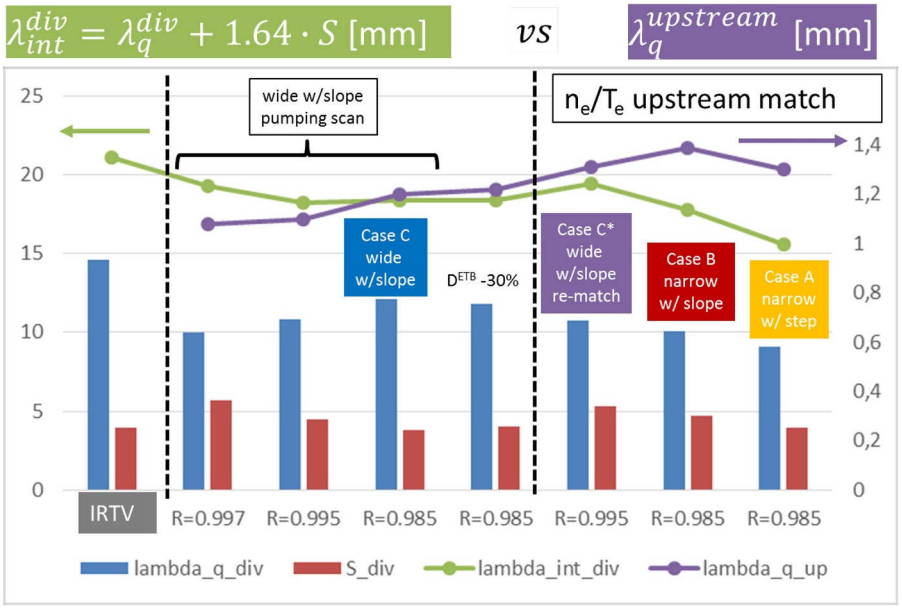

Fig. 5. Comparison of experimental (IRTV) and modelled heat flux parameters by using the Wagner/Eich fitting procedure at divertor entrance λ_q^{div} (neglecting flux expansion) and diffusion parameters S, and the heat decay length directly taken from the mid-plane location λ_q^{up}. The three cases on the right are those cases with matched upstream profiles to the experiment (HRTS), namely case A (yellow), B (red) and C* (purple, c.f. text). The other cases in the middle are scans for recycling coefficient R or modifications in transport. The marked case C (blue) represents the case without any modifications to case A/B but the SOL grid width. (For interpretation of the references to colour in this figure legend, the reader is referred to the web version of this article.)

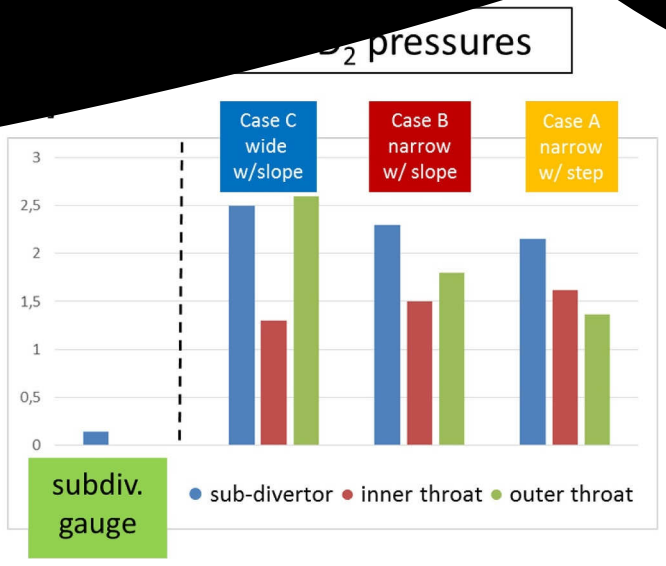

Fig. 7. Modelled molecular pressure p_{D2} at the inner and outer divertor louvre regions (c.f. purple circles in Fig. 3), and at the location of the sub-divertor pressure gauge (red circle in Fig. 3). For comparison the experimental value for the sub-divertor pressure is shown too, showing a massive discrepancy (one order of magnitude) to the modelled p_{D2} (c.f. discussion in text). (For interpretation of the references to colour in this figure legend, the reader is referred to the web version of this article.)

the plasma density in the far-SOL. The re-matched case C* with modified transport/pumping speed lies somewhat in between the two extremes.

4. Discussion

The observations from above can be relatively easy contributed to a change in the neutral distribution when moving from the wide towards the narrower SOL grid width. For the latter (case A/B) neutrals can move more freely across the far-SOL region in the LFS region and may even reach the LFS baffle region above the divertor. From molecular pressure p_{D2} estimates from the model (c.f. Fig. 7) the narrow SOL assumption is not able to compress the neutrals significantly in the LFS. Whilst in the wide SOL grid case (case C) the LFS pressure close to the louvre region is about ~2 larger compared to the HFS louvre, the pressure in cases A/B becomes quite in/out symmetric. Unfortunately, at JET the pressure gauge coverage inside the divertor is practically not existing and the in/out asymmetry in the neutral pressure cannot be compared directly to the experiment. The only sub-divertor pressure gauge measurement available gives pressures way below the expected range of pressure of the order of 1 Pa (c.f. Fig. 7). Whereas the modelled neutral pressure inside the divertor resides in the right ballpark (as it is magni
p_{D2} between t
not expected by the auth
For further assessment the calibration of the
double-checked and the authors concluded that the measurement was correct. The discrepancy for the sub-divertor pressure values for p_{D2} is possibly linked to an overestimate in the neutral conductivity through the louvre structures and hence a too large molecular flux into the sub-divertor. A numerical assessment is currently ongoing (extending the work done by Varoutis and Bonelli [14,15]) in order to identify which of the following neutral transport parameters need to be furtherly constrained: neutral viscosity (BGK option in EIRENE), neutral conductance through the louvres, temperature of walls (thermalizing neutrals). The result of this assessment are to be presented in a future paper.

The narrow SOL grid model assumptions not only produce a quantitative change (lower LFS neutral compression) but also a qualitative change in neutral transport is observed. With no plasma in the way, fast atoms can be easily reflected off the outer vertical divertor plates and hence reach (more indirectly) the region above the X-point. Fig. 8 displays for the narrow and wide grid case a comparison of the ionization source clearly showing the qualitative difference between both cases. With the neutrals being able to be transport further upstream the SOL in the narrow grid case the ionization of particles further upstream requires the energy that leads to a reduction of the $\lambda_{int}^{div}/\lambda_q^{up}$ ratio (with λ_q^{up} staying constant and essentially set by mid-plane transport assumptions).

Table 1 provides as summary of extracted numerical values for outer mid-plane decay lengths for the parallel heat flux, electron temperature and density (λ_q^{up}, λ_{Te}^{up} , λ_{ne}^{up}, respectively). Since a comparison of the numerical profiles to the experimental HRTS profiles was impossible for the far-SOL region (as the errors are too large from this diagnostic in this region) we concentrate only on the near-SOL region. The numerical profiles for n_e and T_e have been fitted to a double-exponential function, thus separating the near-SOL decay lengths from the ones in the far-SOL.

One observes that for the cases in which the upstream T_e^{sep} has been matched (A,B,C*) λ_q^{up} is identical. For all cases, the ratio λ_q^{up} / λ_{Te}^{up} is approximately 1/2. The expected constancy of the ratios λ_q^{up} / λ_{Te}^{up} is preserved as in the two-point model, their exact value however is a factor 7/4 higher compared to the expected value 2/7.

The variation of the near-SOL density decay length λ_{ne}^{up} highlights the impact of the SOL grid extent on the density profile. With the wide grids (C & C*) one observes somewhat steeper near-SOL density decays compared to the cases with a narrow grid (A & B) for which the near-SOL density profile flattens. This flattening is consistent with the extra ionization further upstream in the narrow grid cases (A & B). This is also consistent with the observed increase of the radial particle flow towards

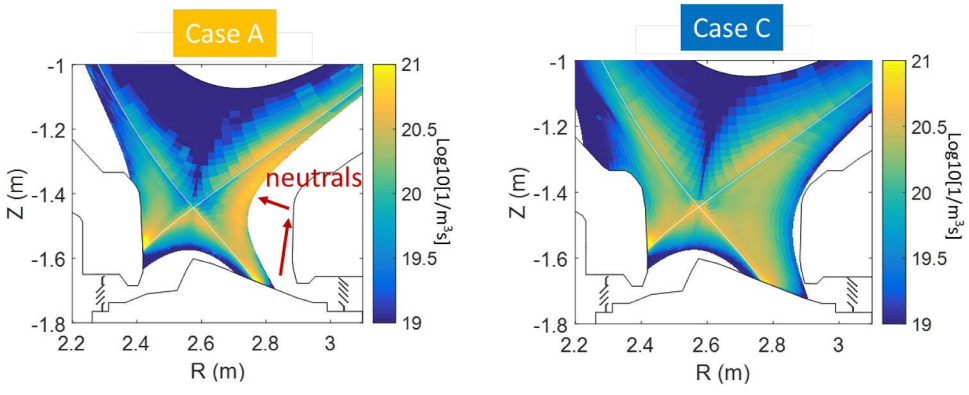

Fig. 8. Left: total ionization source (units: ionizations per volume and time) for case A, right: the same for case C. For case A the typical kinetically reflected pathways for neutrals are sketched, leading to a decrease in the neutral confinement at the LFS and balancing out of in/out neutral pressures. In case A the particle source is enhanced further upstream at the divertor entrance, leading to a stronger cooling in that region compared to case C.

...individual SOLPS-ITER cases (c.f. text

	$\lambda_{q\|\|}$	λ_{Te}	λ_{ne}
A	0,0015	0,0029	0,0092
B	0,0015	0,0030	0,0090
C	0,0013	0,0027	0,0081
C*	0,0015	0,0032	0,0067

the wall in case of the narrow SOL grid. It should be noted that the for the narrow grid cases $\lambda_{ne}^{up} \approx 1$ cm which is just inside the width of the SOL grid upstream ≈ 1.1 cm. As the ration $\lambda_{ne}^{up} / \lambda_{Te}^{up}$ is always > 1 in the investigated cases it holds that $\lambda_{ne}^{up} > \lambda_{Te}^{up} > \lambda_{q}^{up}$ and the limiting factor for the selection of the radial SOL grid extent is λ_{ne}^{up}.

5. Conclusions

It has been demonstrated that for the modelling of the edge plasma conditions for the inter-ELM phase in JET type-I ELMy H-mode discharges with Be/W wall the impact on the finite grid size (i.e. the SOL grid width) cannot be ignored. Especially for more open divertor geometries (i.e. the semi-horizontal divertor configuration) and assuming a too narrow SOL grid width the LFS neutral compression can be significantly underestimated leading to a symmetric in/out neutral pressure equilibration (c.f. also the discussion in [16]). With the neutrals finding a kinetic transport path that increases the particle source further upstream, the heat flux width at the divertor entrance becomes wider due to increased cooling leading to a reduction of the $\lambda_{int}^{div}/\lambda_{q}^{up}$ ratio. Concomitantly, the mid-plane value of λ_{q}^{up} stays always the same and is set by the ratio of radial to parallel conductivities at the mid-plane. By keeping all other transport parameters identical, the SOL grid extending up closer to the wall leads to significantly reduced upstream densities inside the pedestal region and at the separatrix (30% reduction in n_e^{sep}). In such conditions it is possible to increase the density at separatrix and inside the pedestal by modifying numerically the assumption for transport and recycling. However, due to the arbitrariness in such a re-fitting procedure the understanding of the physics (transport, fueling, recycling etc.) becomes blurred. It is obvious that the physics interpretation of the numerical results are subject to the possibility of the modeler's ignorance to the finite grid size issue.

For example, providing input to wall erosion codes like ERO2.0 [7] it is the radial outflow towards the main wall that becomes increased by at least a factor 4–5 if the grid is not extended. The results shown suggest that for calculating the numerical error in the computation of wall erosion fluxes the difference between the two extreme cases (narrow and wide SOL grid width) should be taken as a guideline to estimate the validity of the background plasma.

For the presented simulations it is shown that even for attached conditions the relations $\lambda_{ne}^{up} > \lambda_{Te}^{up} > \lambda_{q}^{up}$ hold. As usually the level of anomalous (particle) transport is not known a priori for interpretative edge plasma simulations one must take the experimental value of λ_{ne}^{up} into account (rather than λ_{q}^{up}) as this is the actual quantity defining the required minimum SOL grid width. In order to avoid numerical artefacts from an unsuitable selection of grid it is recommended to allow for at least factor 2 grid extent in the upstream region compared to the expected density decay parameter λ_{ne}^{up}.

Sometimes, extending the SOL grid width is not possible arbitrarily as the plasma grid in codes like SOLPS-ITER or EDGE2D-EIRENE is technically limited by intersecting baffling structures of the vessel geometry. Some modelers circumvent this issue by modifying the intersecting vessel geometry to allow for a wider plasma grid extent. However this “tweaking” of the grid might lead then to different artefacts, then more related to a change in the kinetic transport of the neutrals when modifying the vessel structure. In the near future, SOLPS-

...is still ...condition ass... other than simply radial ... sheath physics also for the case with grazing ... divertor densities in the investigated H-mode JET discharges, the neutral viscosity does not play a large role and it was shown that small modifications in the divertor wall geometry (e.g. inclusion of a small step in the LFS target plate) only have a minor impact on the overall plasma solutions. It is expected however that with extended grid feature in SOLPS-ITER and/or at higher densities the details in the actual divertor wall structure can be more significant, especially if the simulated (far-SOL) plasma itself is in direct contact with steep edges in the poloidal target tile configuration.

ITER will have a more closed divertor configuration compared to the JET discharge discussed above with strike-lines on both low and high-field side vertical target plates. ITER will operate at higher density with the divertor in a strongly dissipative regime and having partially detached conditions at the LFS divertor induced by Ne or N impurity seeding. Neutral viscosity does also play a role in at elevated densities [17] and the geometric details do matter for the calculating the neutral conductance towards the pump. For ITER relevant edge plasma conditions, an additional study on the impact of the grid size and resolution for N-seeded H-mode JET discharges are currently under way (Ip/Bt = 2.5MA/2.7T at P_{NBI} = 20MW in partial detached conditions with a radiated fraction of ~45%, c.f. [18]). The results of this, numerically demanding, exercise (with a fluid time step $< 10^{-6}$ s) will be presented elsewhere. However, first indications from the ongoing modelling of this JET discharge show that the neutrals in such a closed vertical divertor configuration are much more compressed and any remaining neutral leakage is more related to neutral pathways behind remote areas (c.f. also the work from [5] for Alcator C-mod). In turn the ionization source is kept well inside the divertor volume, closer to the target plates. It is therefore expected that the assumption of λ_{q}^{up} being essentially set by the ratio of radial to parallel heat conductivities at the mid-plane is always a good approximation also for ITER.

All simulations presented here for JET have not been taking into account drift flows. From the experience of modelling of other devices the combined grad-B and ExB drifts leads to a rotation of the flows in clock-wise direction (having the grad-B drift pointing towards the lower divertor). It is expected that by including drift effects the sustained the neutral compression asymmetry (for the wide grid case C a factor ~ 2 in the LFS divertor compared to the HFS divertor) will be somewhat amended leading to a more in/out symmetric neutral pressure distribution. By the time of writing of this paper new H-mode JET simulations including drifts (unseeded conditions for the C30C campaign) are being set up, with the results to be presented elsewhere in the future.

Acknowledgements

This work is in the context of a wider SOLPS-ITER modelling activity towards ITER scale and within the projects done for the ITER Scientist Fellow Network (ISFN). The views and opinions expressed herein do not necessarily reflect those of the ITER Organization. This work has been carried out within the framework of the EUROfusion Consortium and has received funding from the Euratom research and training programme 2014–2018 under grant agreement no. 633053. The views and opinions expressed herein do not necessarily reflect those of the European Commission.

References

[1] M. Wischmeier, J. Nucl. Mat. 415 (2011) S523.
[2] S. Wiesen, J. Nucl. Mat 415 (2015) 480.

[8] S. Wiesen, Nucl. Fusion 57 (2017) 066024.
[9] V. Kotov, Plasma Phys. Control. Fusion 50 (2008) 105012.
[10] F. Wagner, Nucl. Fusion 25 (1985) 525.
[14] S. V
[15] F. Bonelli, N
[16] D. Moulton, Nucl. Fus
[17] A. Kukushkin, Fusion Eng. Des. 86 (2
[18] M. Wischmeier, Proc. IAEA-FEC, Kyoto, Japan, 2016.